# PHYSICAL AND CHEMICAL PROPERTIES AND DURABILITY OF CONCRETE EXPOSED TO COLD CLIMATE FOR OVER 50 YEARS

（Translation from Proceedings of JSCE, No.686/VI－52, September 2001）




Moriaki KUMAGAI　Toshihiko HOSHI　Noboru SAEKI　Toshitaka OHTA

The durability of concrete exposed to cold climate for over 50 years was evaluated by various methods. As the result, it was recognized that the compressive strength of core specimens were remarkable development from 1.8 to 2.0 times compared to that of specimens cured for 28 days at constant temperature in water at the construction. It was originated from that the cement was coarse and was consisted of large amount of belite. The quality of concrete was correspondent to manufacturing performance of the precast concrete, judging from the average neutralization rate coefficient, and it was proven that the good construction was carried out. The degradation by carbonation and so on was limited to the surface layer alone.

***Keywords:*** *concrete durability, long term compressive strength, carbonation, freeze-thaw resistance*

---

Moriaki KUMAGAI is Deputy Director for River and Road Affairs of Kushiro Development and Construction Department, Hokkaido Regional Development Bureau, Ministry of Land, Infrastructure and Transport, Japan. He is a member of JSCE.

---

Toshiko HOSHI is a senior researcher of Research and Development division at Nittetsu Cement Co., Ltd. He obtained B.Eng. from Hokkaido University. His research interests include durability of concrete. He is a member of JSCE.

---

Noboru SAEKI is a Professor of Graduate School of Engineering at Hokkaido University. He obtained his D.Eng. from Hokkaido University in 1972. His research interests durability, FRP, eco-concrete, and reinforced concrete members subject to torsion. He is a fellow of JSCE.

---

Toshitaka OHTA is a Technical Adviser at Nippon Data Service Co. Ltd. in Sapporo. His area of specialization is durability of concrete. He is a fellow of JSCE.

---

## 1. INTRODUCTION

Upon completion of the New Tokachi Bridge, the first Tokachi Bridge opened to traffic in 1941 was taken out of service after more than 50 years. Meteorological conditions in Obihiro located of the bridge, are harsh in winter, with minimum temperatures dropping below −20 ℃ from time to time. Nevertheless, the concrete of the bridge remained in satisfactory condition despite exposure to this severe environment for over half a century. A decision was made to use the concrete for an exposure test that would cover 200 years from construction, an unprecedented time span for such testing at Bibi in Chitose City, Hokkaido. In this way, the bridge will continue its contribution to society for many years to come.

This long−term exposure test, proposed by TC: Investigation into durability of the Tokachi Bridge (Chairman: Noboru Saeki), will prove very significant in evaluating concrete durability. Follow−up surveys on durability will be conducted every five years until 2141. This report describes properties of concrete after the 50−odd years of service, which corresponds to initial values for the long−term exposure test that will last a further 150 years.

## 2. CONCRETE AT CONSTRUCTION TIME [1] [2]

(1) Materials

a) Cement

The substructure and superstructure concrete work for the Tokachi Bridge were carried out between November 1935 and October 1937 and between September 1938 and November 1939, respectively. Construction seems to have taken place at a time when cement quality was undergoing significant changes in Japan. According to an examination by the Civil Engineering Laboratory, Ministry of Internal Affairs, cement strength began decreasing in FY 1938, and the strength of cement produced in FY 1940 was approximately 80% that of FY 1937 [3]. This was caused by inferior coal combustion, resulting in larger amount of free lime and aluminium oxide in the cement; that is, these were a decrease in tricalcium silicate, accompanied by an increase in tricalcium aluminate and coarser powder. Although cement quality differed by cement factories and time of production, it is believed that the cement used for the Tokachi Bridge was also of reduced strength.

b) Aggregate

The sand was taken from the Tokachi River, and the specific gravity and water absorption of this aggregate are 2.65 and 1.5%, respectively. On the other hand, the gravel was sourced from the Satsunai River, with a specific gravity and water absorption of 2.67 and 0.83%. Its maximum size is 25 mm. Although aggregate from both rivers contains considerable amounts of organic matter, it was considered suitable for the bridge.

(2) Mix proportions

With the allowable compressive strength of concrete used for bridge superstructure work being 6.4 $N/mm^2$, mix proportioning strength was specified as 22.0 $N/mm^2$, namely, three times the allowable compressive strength plus 15% to take into account variations in the quality of concrete at construction sites. The detailed Specification for highway structures in 1926 stipulated that mix proportion of concrete for bridge should be cement 1 : sand 2 : gravel 4 by volume and that characteristic compressive strength of concrete should be 13.7 $N/mm^2$. It was also stipulated that 300 $kg/m^3$ was required as the minimum unit cement content in order to prevent from corrosion of embedded steel.

For the superstructure concrete, mix proportion tests with different water−cement ratios and sand−gravel mixing ratios were conducted, and the specified mix was determined by taking into account substructure (abutments, piers) concrete strength test results, the use of internal vibrators during placement, etc.

**Table 1** describes the specified mix proportions of the Tokachi Bridge concrete. For the substructure concrete, the mix proportion was fundamentally determined according to the detailed Specification for highway structures and modifications were made to satisfy strength requirements through tests.

**Table 1** Specified mix proportions of concrete

| | Mix proportioning strength ($N/mm^2$) | Mix proportion (volume) C : S : G | Water-cement ratio (weight) (%) | Unit Content ($kg/m^3$) C : S : G | Remarks |
|---|---|---|---|---|---|
| Beam<br>Slab | 22.0 | S/G=0.3/0.7 | 52 | 330 559 1365 | Ordinary portland cement |
| Abutment<br>(Support) | 13.7<br>19.1 | 1 : 1.92 : 3.83<br>1 : 1.69 : 3.38 | 55 − 60<br>50 − 55 | 300<br>330 | Ordinary portland cement |
| Pier<br>(Support) | 13.7<br>19.1 | 1 : 1.92 : 3.83<br>1 : 1.62 : 3.38 | 55 − 60<br>50 − 55 | 300<br>330 | Ordinary portland cement |

(3) Compressive strength

**Table 2** shows the compressive strength of the concrete beams. As indicated in **Figure 1**, the average strength of the concrete in Span 7, which is the one subject to long−term exposure testing, after moist curing for 28 days at temperature between 18 ℃ and 24 ℃ was 23.0 $N/mm^2$. It thus satisfied the mix proportioning strength. It is thought that the strength of the concrete in Span 5, which was placed in 1938, is higher than that of other spans, which were placed in 1939, due to the influence of cement quality.

**Table 2** Compressive strength of concrete (Anchored Beam) at construction time

| Span | Type | Slump (cm) | Compressive strength ($N/mm^2$) | | | | Period of construction |
|---|---|---|---|---|---|---|---|
| | | | 7−day | | 28−day | | |
| | | | Atomospheric curing | Moist curing | Atomospheric curing | Moist curing | |
| Span 5 | Beam | 11.5 | 16.5(18) | 18.5(18) | 25.3(18) | 32.4(18) | |
| | Slab | 8.5 | 14.9(12) | 21.3(12) | 24.8(12) | 28.7(12) | |
| | Support | 11.0 | 12.2(6) | 17.4(6) | 24.3(6) | 28.2(6) | |
| | Average | 10.3 | 15.2 | 19.3 | 25.0 | 30.5 | Sep.10−Oct.14, 1938 |
| Span 7 | Beam | 10.3 | 8.8(8) | 11.8(8) | 16.7(8) | 25.5(4) | Oct.12−Oct.21, 1939 |
| | Slab | 11.1 | 9.8(2) | 13.7(2) | 19.6(6) | 22.5(4) | Oct.26−Oct.28, 1939 |
| | Support | 10.7 | 10.8(6) | 13.7(6) | 15.7(4) | 20.6(3) | Nov.9−Nov.9, 1939 |
| | Average | 10.7 | 9.6(16) | 12.7 | 17.0 | 23.0 | |
| Span 9 | Beam | 8.6 | 8.8(19) | 13.7(19) | 14.7(20) | 21.6(12) | Apr.3−Apr.17, 1939 |
| | Slab | 10.5 | 9.8(3) | 11.8(2) | 19.6(7) | 22.5(6) | Apr.22−Apr.26, 1939 |
| | Support | 7.7 | 12.7(2) | 14.7(2) | 21.6(2) | 24.5(2) | Apr.30−May 1, 1939 |
| | Average | 8.9 | 9.3 | 13.6 | 16.7 | 22.1 | |

Figures in parentheses indicate the number of test specimens.

## 3. CONCRETE CORE SAMPLING LOCATIONS

Core specimens were collected at the locations described in **Figure 1** with the aim of elucidating the impact of environmental conditions on the concrete. For the superstructure, samples were taken from three beams of Span 7, the outer upstream beam (Beam 5), the center upstream beam (Beam 4) and the middle beam (Beam 3). For the substructure, specimens were sampled horizontally from the in−air, wet and dry, and underwater areas of pier P7 (e). For the slab ((b) shadowed portion), sampling was carried out vertically, and as an underground sample, specimens were collected horizontally from the A2 abutment (f). Aiming to ascertain the state of construction joint, sampling was conducted vertically from the upper part of the center beam (Beam 3, vertical). The basic core dimension was set at $\phi$ 150×L mm.

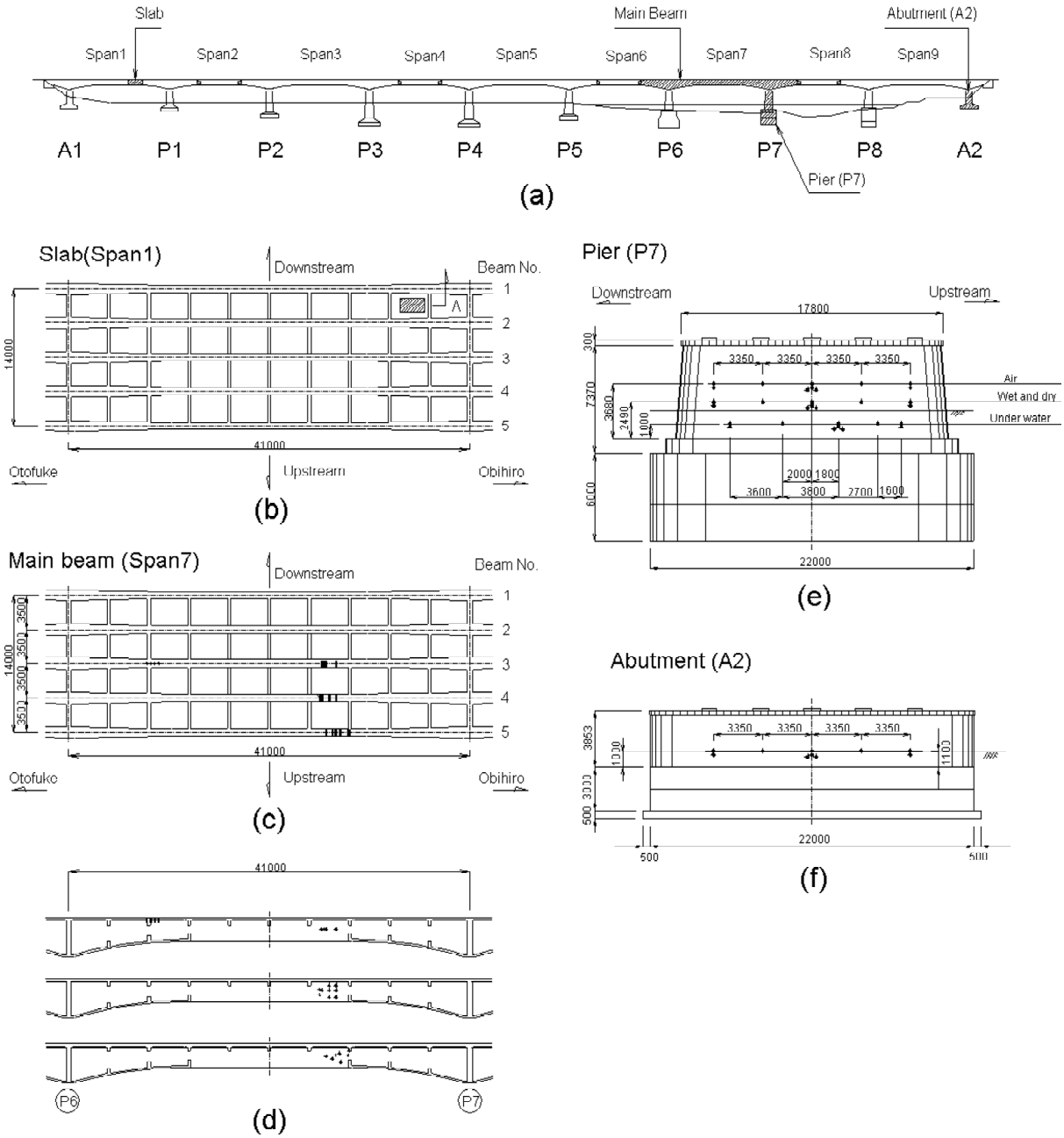


**Fig. 1** Core sampling locations

## 4. TEST METHODS

(1) Optical microscope

In order to grasp the burning and hydration conditions of the cement clinker, reflecting and polarizing microscope observations were conducted. In addition, identification of aggregate rock types was also performed.

(2) Chemical analysis

Chemical analyses of hardened paste sampled from the slab were conducted in conformity with JIS R 5202 to determine the chemical composition of the cement.

(3) Air void system

Air contents and spacing factors were measured using 300−350 mm slices taken from the core surface, in conformity with ASTM C 457 by the linear traverse method.

(4) Bulk density of concrete and compressive strength

Test specimens of $\phi$ 150 mm×300 mm were allowed to absorb water for 48 hours. Consequently, the bulk density of concrete was measured according to JIS A 1110 and compressive strength tests were carried out in conformity with JIS A 1107.

(5) Neutralization

Neutralization tests were performed on the basis of the color reaction of a 1% phenolphthalein ethanol solution, and depth of neutralization was expressed as the distance up to florid parts (pH=10 or more). Average depth of neutralization refers to the average distance obtained by measuring at 10 mm intervals.

(6) X−ray diffraction

Powder X−ray diffraction were performed with the aim of identification and semi−quantification of the hydration products of cement and new products. Three samples (0−20 (10), 40−60 (50), 90−110 (100) mm) were used. After being pulverized in acetone, mortar was dried in a nitrogen gas flow at normal temperature for 24 hours and then put through a 74 μm sieve to obtain powder. To perform the semi−quantitative analysis, 10% of magnesium oxide (MgO) was added to the samples, those mixed samples were then ground by vibro−mill. The main diffraction peak intensity was corrected by (1+100) by hydrochloric acid insoluble residue of powder which put through a 74 μm sieve. The produced quantity was evaluated by relative peak intensity vis-a-vis MgO on a paste basis.

The tests were carried out with RINT−2200 X−ray diffraction equipment using the Cu−Kα wave length (40 kV tube voltage; 40 mA tube current) through a Ni filter. The scanning rate and scanning step of the goniometers were set at 0.3°/min and 0.01°, respectively.

(7) Thermal analysis (DTA−TG)

Powder that passed the 74 μm sieve for use in X−ray diffraction was used. TAS−200 thermal analysis equipment was used for the analysis and measurements covered the range 20−1000 ℃ in an argon gas atmosphere (50 cc/min flow rate) at the programmed rate of 10 ℃/min. With regard to the quantification of products, a (1+100) hydrochloric acid insoluble residue correction was performed on a paste basis.

(8) Infrared absorption spectral analysis

The infrared absorption spectral analysis was performed by the KBr tablet method, using the same powder samples as in the thermal analysis. A FT/IR−230−S analyzer was used.

(9) CMA

Aiming for quantification of major components at the concrete surface and $CaO/SiO_2$ mole ratio, analysis using a CMA (Computer−aided X−ray Micro Analyzer) was performed using a CMA JXA8900. Analysis conditions included an acceleration voltage of 15 kV and an irradiation current of 0.1 μA, and analysis covered an area of 20×20 mm, with one pixel measuring 40×40 μm.

(10) SEM−EDS

In order to observe product morphology and gain an understanding of product identification by elementary analysis as well as the product generation process, samples were spattered with silver and were then observed and analyzed at an acceleration voltage of 15 or 20 kV and with a 100 nm beam diameter using the JSM−840/EDS scanning electronic microscope equipped with energy dispersive analysis equipment. Sampling locations were the same as those used for X−ray diffraction.

(11) Pore size distribution

The measurement pore size distribution was carried out by the mercury intrusion method and the nitrogen adsorption method in order to quantify the capillary pores and gel pores in the concrete. Samples were prepared by conditioning the mortar into lumps measuring 2−5 mm by nippers, and these were then D−dried for 7 days.

An Autopore III 9420 was used for the mercury intrusion method and pores 3 nm−342 μm in diameter (3.65 kPa−411 MPa) were analyzed. For the Washburn equation, 130° and 485 dynes/cm were used as the mercury contact angle and surface tension, respectively.

For the nitrogen adsorption method, an Asap−2400 was used to analyze pores 1−300 nm in diameter.

(12) Freeze−thaw tests

The freeze−thaw resistance of the concrete was investigated by carrying out underwater freeze−thaw tests according to JSCE−G 501−1986. Core specimens for testing were collected from Beam 5, pier P7 (in−air, wet and dry, and underwater areas), and below ground at the abutment. Test specimens were cut into 10×10×40 cm by avoiding reinforcing bars from the core. Tests were initiated by allowing the test specimens to absorb water for 48 hours.

## 5. PHYSICAL AND CHEMICAL PROPERTIES OF CONCRETE

(1) Concrete materials

a) Cement clinker

The following findings were obtained as a result of optical microscope observations of the pier in−air, Beam 3, and floor slab ((b) shadowed portion) samples as in **Figure 1**.

The cement clinker of the pier in−air sample contains well−developed automorphic (hexagonal) fine alite ($3CaO \cdot SiO_2$). The interstitial phase content is generally low.

Large amount of belite ($2CaO \cdot SiO_2$) are contained as clusters. However, the properties of belite differ from cluster to cluster, with a total of four types of cluster having various thermal histories, ranging from inferior to favorable burning conditions.

① Belite derived from clinker under favorable burning and cooling conditions is large in size and the type I cross lamella (α → α' transformation texture) is well developed (**Photo 1**).
② Belite in clinker that was annealed in the kiln retains cross lamellae in the crystal center alone, and lamellae in peripheral areas have disappeared. This may be because the cooling rate is low inside large clinker.
③ For more annealed clinker, the type II (α'→ β transfer convergent twin crystal textures) parallel lamellae have developed outside the belite crystal.
④ Belite in clinker made under inferior burning and cooling conditions is small in grain size and irregular in shape.

**Phot. 1**

The interstitial phase is coarse and its distribution is not uniform. Aluminate ($3CaO \cdot Al_2O_3$) stands out in some cement grains while ferrite ($4CaO \cdot Al_2O_3 \cdot Fe_2O_3$) is prominent in other cement grains. It may therefore be concluded that the cement clinker used for the piers were made from raw material particles of ununiform size and were burned insufficiently. It is also inferred that smaller amount of alite and larger amount of belite than in the design composition were

composed due to insufficient reaction of forming clinker.

Regarding alite in the Beam 4, fine non-hydrated clusters of automorphic crystals are recognized. Belite is mainly of the following two types:

① Type I belite with clear cross lamellae, indicating high-temperature burning and rapid cooling.
② Slightly unclear cross lamellae with some belite annealed in a kiln or large-grain clinker.

These account for the majority of the belite and crystal grain sizes are relatively uniform. Therefore, the clinker indicates that high-temperature burning and rapid cooling were performed using a stable process. The generally fine interstitial phase (low content) indicates that the clinker was rapidly cooled within a cooler. These are prerequisites for enhancing cement quality (strength). As belite is generally the component that determines long-term cement strength development, high-quality belite is regarded as contributing to the long-term strength of concrete.

For floor slab A, favorably burned and cooled clinker was used. The belite in the clinker is of three types:

① Belite with cross lamellae and indication of high-temperature burning and rapid cooling.
② Belite with cross lamellae becoming somewhat unclear.
③ Belite surrounded by lamella-free, petaline belite with some indicating annealing in the kiln.

Nevertheless, type ① is prevalent. Interstitial aluminate and ferrite are fine, indicating that they were thoroughly cooled. It is presumed, therefore, that the cement quality was good.

The following three findings resulted from the microscope observation of pier, beam, and slab cores:

① Cement was coarse, with a maximum grain size of 200-300 μm.
② The cement used for piers had a range of burning and cooling conditions
③ The cement used for beams and floor slabs was of higher quality than that used for piers

b) Mineral composition of cement

**Table 3** describes the chemical and mineral composition of the cement (paste) inadvertently remaining as lumps in the floor slab core.

**Table 3** Presumed chemical and mineral composition of cement (%)

| | $SiO_2$ | $Al_2O_3$ | $Fe_2O_3$ | CaO | MgO | $SO_3$ |
|---|---|---|---|---|---|---|
| | 23.36 | 5.22 | 2.84 | 64.36 | 1.90 | 1.35 |
| By Bogue method | | C3S | C2S | C3A | C4AF | Gypsum |
| | | 41 | 36 | 9 | 9 | 3 |

Although the cement can be described as portland cement, alite and belite account for 41% and 36%, respectively. That is, it is similar to current moderate-heat portland cement with low early strength, and long-term increases in strength can be expected.

c) Aggregate

The fine aggregate is river sand consisting of quartz grains, feldspar grains, pyroxene grains, amphibole grains, sedimentary rock (slate etc.), volcanic rock (vitreous), volcanic ash (pozzolan), etc. Although it is stated that volcanic rock (vitreous) can increase the possibility of alkali-aggregate reaction, alkali-aggregate reaction was not found in this survey.

The coarse aggregate is river gravel consisting primarily of sedimentary rock (sandstone), as well as metamorphic rock, volcanic rock, etc. so it mostly has a flat shape (short axis/long axis=0.46-0.60).

(2) Physical properties of concrete

a) Bulk density of concrete

**Table 4** shows the results of measuring each core specimen's density. The density of concrete was 2.40 t/m$^3$ or greater, significantly more than that of general concrete, which is 2.3−2.4 t/m$^3$. Although the figures for Beam 3 (vertical) are slightly low, this is thought to have been caused by bleeding and other effects because the sampling location was on the upper face of members.

**Table 4** Bulk density of concrete (t/m$^3$)

| | Slab | Beam 5 | Beam 4 | Beam 3 | Beam 3 (vertical) | Pier P7 | Abutment |
|---|---|---|---|---|---|---|---|
| Av. value | 2.44 | 2.46 | 2.46 | 2.44 | 2.41 | 2.46 | 2.44 |
| Min. value | 2.44 | 2.42 | 2.43 | 2.42 | 2.40 | 2.40 | 2.42 |
| Max. value | 2.46 | 2.49 | 2.48 | 2.46 | 2.43 | 2.50 | 2.45 |

As the external appearance of each core was dense and few large voids were recognized, it is apparent that the concrete was sufficiently compacted with its denseness and uniformity.

b) Air content

**Table 5** indicates the air content of the concrete. The air content of slabs and beams was 0.60% and 0.72−1.70%, respectively, and that of piers and abutments was 0.45−0.65% and 2.30%, respectively. Regardless of location, the air content was low, which indicates that the concrete used non−AE concrete. In the case of that the maximum size of coarse aggregate is 25 mm, the amount of entrapped air is normally expected to be 1.5%. However, some sections of the core contain less than 1% of air, suggesting that sufficient compaction was performed.

**Table 5** Air content (%)

| Slab | Beam 5 | Beam 4 | Beam 3 | Beam 3 (vertical) | P7 in−air | P7 wet and dry | P7 underwater | Abutment |
|---|---|---|---|---|---|---|---|---|
| 0.60 | 0.72 | 1.64 | 1.02 | 1.70 | 0.50 | 0.65 | 0.45 | 2.30 |

c) Compressive strength

**Table 6** indicates the compressive strength distribution. The average strength, standard deviation, and coefficient of variation of the main beam concrete were 46.1 N/mm$^2$, 8.6 N/mm$^2$, and 18.3%, respectively. The range of strength was twofold from 23.0 N/mm$^2$ (Span 7 concrete of moist curing for 28 days) to 46.1 N/mm$^2$. Although the strength of the Beam 5 is lower than that of the Beam 3, whether this was due simply to qualitative unevenness or differences in exposure conditions remains unknown.

**Table 6** Compressive strength frequency table

| Compressive strength (N/mm$^2$) | Slab | Beam 5 | Beam 4 | Beam 3 | Beam 3 (vertical) | Pier P7 | Abutment |
|---|---|---|---|---|---|---|---|
| 25 − 30 | | 1 | | | | 1 | |
| 30 − 35 | | 1 | | | | 2 | |
| 35 − 40 | | 3 | | | 1 | 4 | 1 |
| 40 − 45 | | 1 | | 1 | 1 | 6 | |
| 45 − 50 | 1 | | | 1 | 1 | 2 | 2 |
| 50 − 55 | | 4 | 3 | 1 | 1 | | 1 |
| 55 − 60 | 1 | | 1 | 1 | 1 | | 1 |
| 60 − 65 | 1 | | | | | | |
| Av. value | 55.2 | 42.7 | 54.1 | 50.3 | 46.8 | 39.5 | 48.3 |

Although the bridge piers and abutments have the same mix proportion and they were constructed within a relatively narrow time frame − March−April and September−October, 1937 − there was a significant difference in average compressive strength after 28 days of moist curing: 22.2 N/mm$^2$ and 27.0 N/mm$^2$.

The average core strengths were 39.5 N/mm$^2$ and 48.3 N/mm$^2$, respectively, so the cores clearly inherited the impact of differences in strength at the time of construction. The strength development during the service period for both was 1.8 times.

(3) Texture of concrete

a) Pore structure by nitrogen adsorption method

The specific surface areas of samples from slabs and beams of the superstructure are 10.76 and 6.73−16.98 m$^2$/g, respectively, whereas those from piers and abutments of the substructure are 28.0−31.8 and 25.71 m$^2$/g. Specific surface area can be considered on index describing degrees of texture elaborateness, and the more elaborate the texture, the smaller the specific surface area is. Superstructure concrete is smaller in specific surface area and denser in texture than substructure concrete, and these differences are believed to be manifested as differences in compressive strength.

The pore volume of slabs, beams, piers, and abutments is 0.0209, 0.0113−0.0199, 0.0311−0.0549, and 0.043 ml/g, respectively. As with specific surface area, there are clear distinctions in concrete texture between superstructure and substructure.

b) Optical microscope observation

Concrete commonly contains large amounts of vitreous volcanic ash that is derived from the fine aggregate, and it is acknowledged that this can cause a marked pozzolanic reaction with cement. The hydration of cement in concrete is thought to have been accelerated by pozzolanic reaction in this case, and it is thus thought that the development of high strength is partially attributable to the presence of volcanic ash.

(4) Factors of increasing in concrete long−term strength

When concrete is thoroughly cured, long-term increases in strength are observed, particularly in the belite, and coarse−grained cement with low early strength is said to be advantageous. The cement in the Tokachi Bridge contains large amounts of belite. In addition, as it is coarse with the maximum grain size of 200−300 μm, it was especially suitable for promoting strength over a long period of time. Furthermore, similar increases in strength can be found even in cement whose burning conditions were not favorable. Volcanic ash originating from the fine aggregate is also considered to have promoted the hydration of cement through long−term pozzolanic reaction.

Differences in texture, density, and strength between superstructure and substructure are considered as indicative of differences in burning conditions of the cement.

## 6. PHYSICAL AND CHEMICAL PROPERTIES RELATING TO DURABILITY

Physicochemical tests were performed on cores taken at the same location as cores sampled for compressive strength tests. Other than for neutralization results, however, the results given here focus on the cores from the Beam 4, the Beam 5, and pier P7 in−air and wet and dry areas. In the case of freeze−thaw resistance, specific core results are stated.

(1) Neutralization

**Table 7** gives the neutralization test results. It is reported that the passive film on reinforcing bars is destroyed [4] at pH 9 or below and corrosion then advances. Since the maximum depth of neutralization is important in considering the corrosion of reinforcing bars, comparisons are made on the basis of this measure. The figures for Beam 3 (vertical), which serves as the construction joint, and the abutment underground area were small at 0 and 3 mm, respectively, whereas those for slabs, piers, and bridge beams exposed to air and water were large at 25, 15−32, and 16−20 mm, respectively.

**Table 7** Neutralization test results

| Location | Depth of neutralization (mm) | | | Neutralization rate coefficient ($mm/year^{1/2}$) | |
|---|---|---|---|---|---|
| | Minimum | Maximum | Average | Maximum | Average |
| Slab | 6 | 25 | 14.4 | 3.3 | 1.9 |
| Beam 5 | 20 | 32 | 26.4 | 4.3 | 3.5 |
| Beam 4 | 10 | 22 | 17.6 | 2.9 | 2.4 |
| Beam 3 | 1 | 15 | 4.7 | 2.0 | 0.6 |
| Beam 3 (vertical) | 0 | 0 | 0.0 | | |
| P7 in-air | 1 | 20 | 7.1 | 2.7 | 1.2 |
| P7 wet and dry | 5 | 16 | 10.0 | 2.1 | 1.3 |
| P7 underwater | 3 | 20 | 8.9 | 2.7 | 0.9 |
| Abutment underground | 0 | 3 | 0.7 | 0.4 | 0.1 |

This is because the Beam 3 (vertical), a construction joint, was exposed to air only for a short period of time during construction, and the underground area had no contact with hazardous hot spring water or other substances that cause neutralization.

Generally, neutralization rate is affected by humidity and it reaches its peak when the relative humidity is 50-70%. The rate decreases again as humidity rises above 70% until it becomes almost nil at 100%. Nevertheless, the depth of neutralization at the pier's in-air, wet and dry, and underwater areas is almost identical. This suggests that there was a period during the past 50-odd years in which different parts of the concrete were exposed to air due to water level fluctuations and changes in water flow caused by riverbed scouring.

Of locations exposed to air, the Beam 5 have the largest depth of neutralization, presumably because loosening of the concrete texture by wintertime freeze-thaw action expedited neutralization.

The depth of neutralization "d" is proportional to the square root of the number of years elapsed "t", a relationship that expressed as $\mathbf{d=Kt^{1/2}}$. **Table 7** indicates values of coefficient **K** obtained from depth of neutralization by assuming that the time elapsed was 56 years. This coefficient is a constant determined by concrete quality and the exposure environment [5]. It is thus possible to make an evaluation of concrete quality using this coefficient. Menzies et al. [6] reported on correlations between average neutralization rate coefficient and concrete manufacturing conditions (for prestressed concrete, precast concrete, and cast-in-place concrete) as well as correlations between the mean depth of neutralization and compressive strength based on 54 year experiments. If those correlations are applied to these test results, it is possible to judge that the slabs, beams, and piers, excluding the Beam 5, correspond to the manufacturing conditions of precast concrete (**K** being 3 or below). In addition, the compressive strength of the concrete core is equivalent to the 45-50 $N/mm^2$ category (cubic test specimens).

If we estimate the depth of neutralization in 150 years' time (206 years after construction) based on the maximum neutralization rate coefficient, it will increase by 1.9 times the current depth to 29-61 mm, exception in the underground area of the bridge abutment. Although concrete from the Beam 3 will be used for durability tests over the next 150 years, the neutralization front is expected to reach the reinforcing bars in 100 years because the cover over the reinforcing bars is 25 mm.

(2) X-ray diffraction

**Figure 2** shows examples of X-ray diffraction patterns. Minerals identified by X-ray diffraction include belite (derived from cement), calcium hydroxide ($Ca(OH)_2$), which is a hydration product, calcium aluminate hydrate ($3CaO \cdot Al_2O_3 \cdot 6H_2O$), monosulphate ($3CaO \cdot Al_2O_3 \cdot CaSO_4 \cdot 12H_2O$), and calcium silicate hydrate with low crystallinity ($xCaO \cdot ySiO_2 \cdot zH_2O$, wide peak of approx. $2\theta=30°$). Furthermore, calcite ($CaCO_3$) and vaterite ($CaCO_3$) with different lattice constants were confirmed as new products.

**Figure 3** describes the relationship between distance from concrete surface and the relative peak intensity

of products (diffraction peak intensity ratio of products vis-a-vis the diffraction peak intensity of MgO, added in specific amounts). A comparison of the calcite quantity produced at a depth of 10 mm indicates that the P7 wet and dry area had the largest quantity, followed by the Beam 5, the P7 in−air area, and the Beam 3. Vaterite was generated in the P7 cyclic wet and dry section as well as the Beam 4, indicating that it exists in cores where calcite abounds. Based on these findings, the generation of vaterite can be regarded as a index of carbonation degree. Stark and Ludwig [7] reported that vaterite was generated by the carbonation of calcium silicate hydrate with a low $CaO/SiO_2$ mole ratio and monosulphate. This indicates that it reveals the carbonation of calcium silicate hydrate and monosulphate.

The quantity of calcium hydroxide generated was maximum at 50 mm in the Beam 5, the P7 in−air and wet and dry areas, which suggests at the transfer and deposition of calcium ions from inner potion.

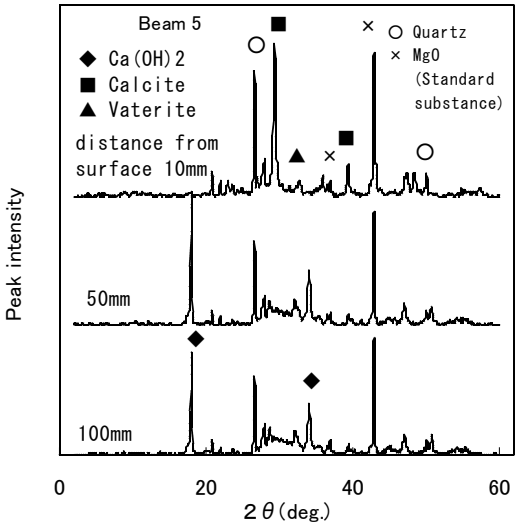


**Fig 2** X-ray diffraction patterns

(3) Thermal analysis

**Figure 4** and **Table 8** present examples of differential thermal analysis curves and the minerals identified, respectively. Gypsum was confirmed at 10 mm in the Beam 3, the P7 in−air area, and in the wet and dry area, whereas ettringite was confirmed at 10 mm in the Beam 3 and in the P7 in−air area. The only locations where monosulphate was not confirmed were at 10 mm in the Beam 5, the Beam 3, and in the P7 wet and dry area.

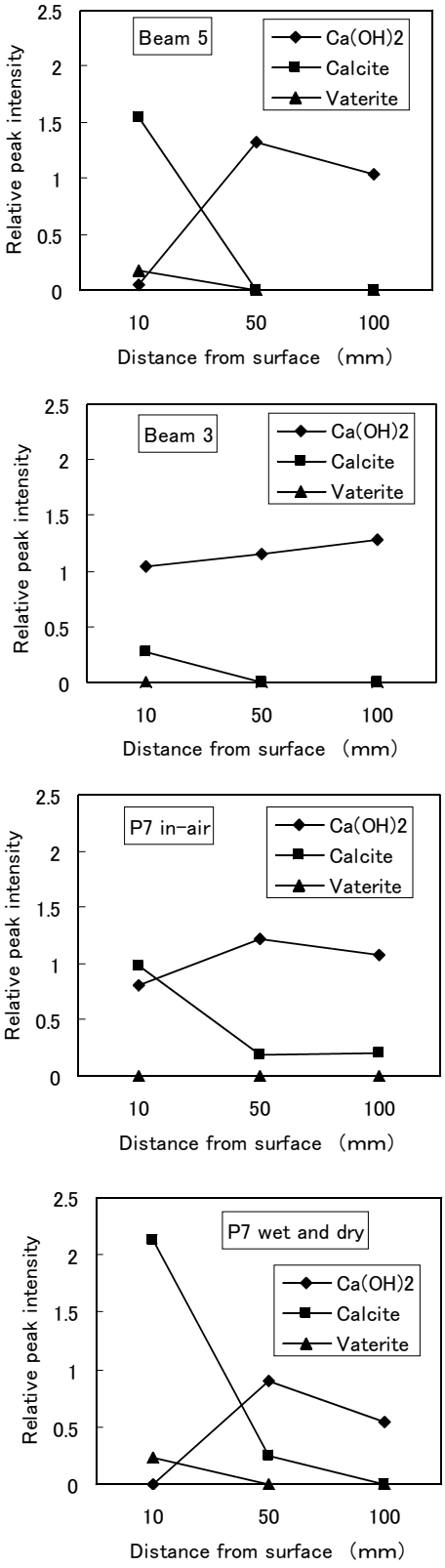


**Fig. 3** Relationship between distance below surface and relative peak intensity of each product

Calcium hydroxide was not confirmed only at 10 mm in the P7 wet and dry area. Calcium carbonate was confirmed at all locations. **Figure 5** describes the relationship among distance from the surface and quantity of calcium carbonate and calcium hydroxide generated. A comparison of calcium carbonate quantity generated at a depth of 10 mm indicates that the P7 wet and dry area generated most, with 57%, meaning that carbonation is most advanced there. Calcium hydroxide tends to be low in quantity in the surface layers but higher in quantity in inner regions. Although the Beam 4 and Beam 5 have slightly different trends in calcium hydroxide in the X-ray diffraction results, a comparison of the quantity generated by depth reveals that there is a peak at 50 mm, except in the case of the Beam 5. This indicates a transfer and deposition of calcium ions from inner portion. The P7 wet and dry area indicates lower calcium hydroxide quantity than other cores even in inner regions, indicating that dissolution has reached the inner regions.

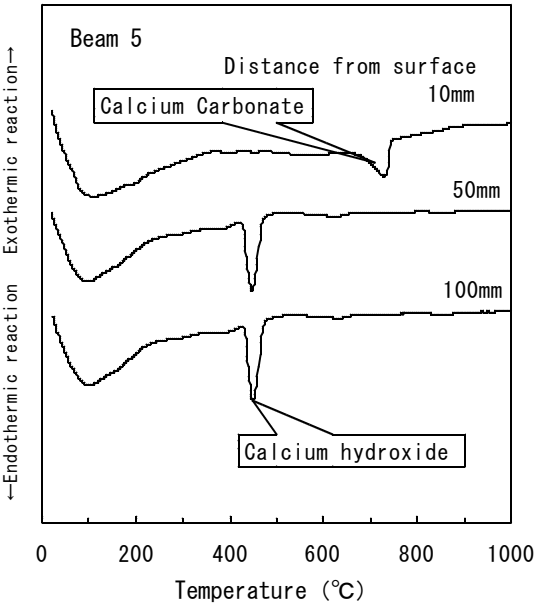


**Fig. 4** Differential thermal analysis curves

**Table 8** Identified minerals

| | Distance from surface (mm) | Gypsum | Ettringite | Monosulphate | Calcium hydroxide | Calcium carbonate |
|---|---|---|---|---|---|---|
| Beam 5 | 10 | | | | ○ | ○ |
| | 50 | | | ○ | ○ | ○ |
| | 100 | | | ○ | ○ | ○ |
| Beam 3 | 10 | ○ | ○ | | ○ | ○ |
| | 50 | | | ○ | ○ | ○ |
| | 100 | | | ○ | ○ | ○ |
| P7 in-air | 10 | ○ | ○ | ○ | ○ | ○ |
| | 50 | | | ○ | ○ | ○ |
| | 100 | | | ○ | ○ | ○ |
| P7 wet and dry | 10 | ○ | | | | ○ |
| | 50 | | | ○ | ○ | ○ |
| | 100 | | | ○ | ○ | ○ |

Stark and Ludwig [8] have reported that carbonation causes partial decomposition of monosulphate into aluminum hydroxide ($Al(OH)_3$), gypsum ($CaSO_4 \cdot 2H_2O$), and calcium carbonate, and that the gypsum then reacts with non-carbonated monosulphate to generate ettringite. It is considered, therefore, that the gypsum and ettringite existing at 10 mm are attributed to the carbonation of monosulphate.

(4) Infrared absorption spectrum analysis

**Figure 6** shows infrared absorption spectrums for the P7 wet and dry area. At 50 and 100 mm, the absorption due to the OH stretching vibration of calcium hydroxide was found at 3634 $cm^{-1}$, and that due to the $SiO_4^{4-}$ stretching vibration of calcium silicate hydrate was confirmed at 980 $cm^{-1}$, which suggests a high $CaO/SiO_2$ mole ratio. In contrast, at 10 mm, the absorption caused by the OH in calcium hydroxide disappeared and the

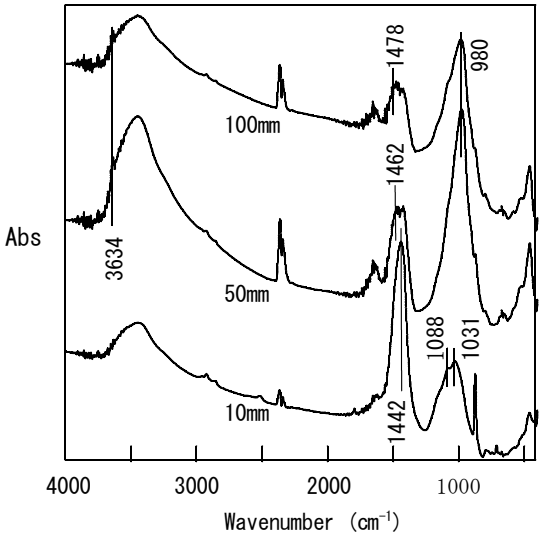


**Fig. 6** Infrared absorption spectrum

absorption peak due to $SiO_4^{4-}$ of a calcium silicate hydrate had shifted to 1031 $cm^{-1}$. This indicates a low $CaO/SiO_2$ mole ratio. Further, absorption considered to be caused by silica gel [9] was confirmed at 1088 $cm^{-1}$ (the shoulder peak). Absorption due to the $CO_3^{2-}$ asymmetrical stretching vibration of calcium carbonate had shifted to 1442 $cm^{-1}$ in the surface layer and approximately 1470 $cm^{-1}$ in inner regions, and the absorption was greater in the surface layers than in inner regions. It is thought that, at 10 mm, calcium hydroxide changes into calcium carbonate and that calcium silicate hydrate also has a low $CaO/SiO_2$ mole ratio through carbonation. Silica gel is produced by the further decomposition of the calcium silicate hydrate with a low mole ratio.

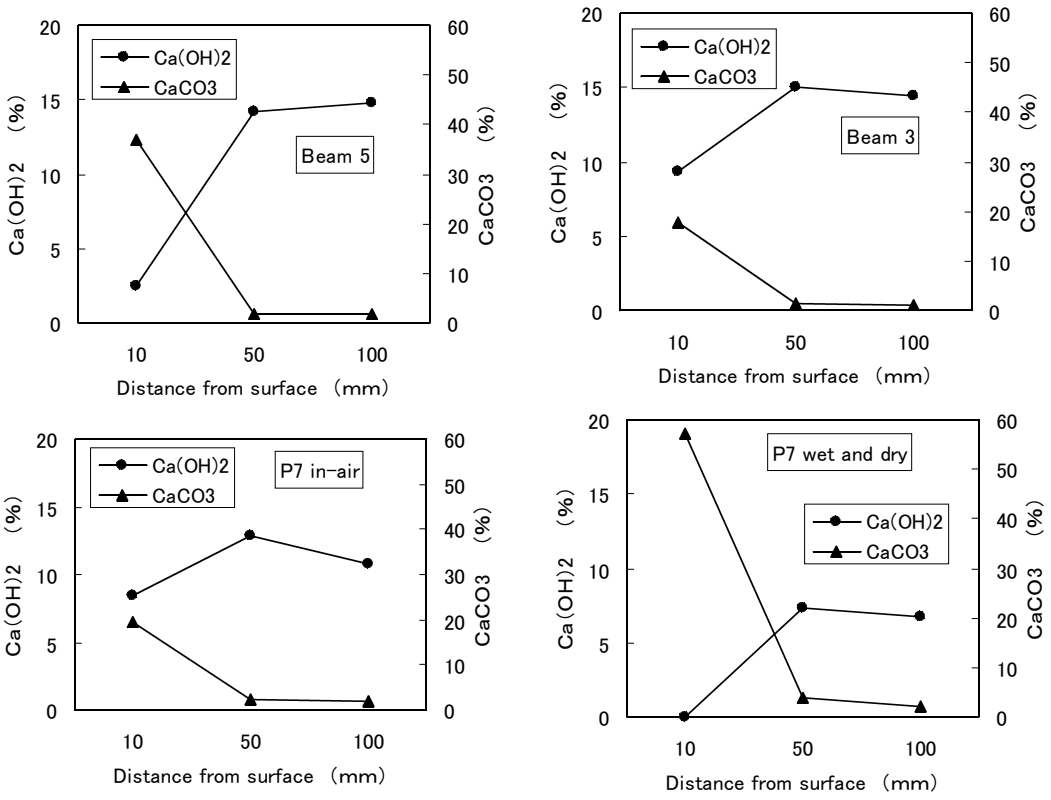


**Fig. 5** Relationship between distance below surface and volume of products generated

(5) CMA

**Figure 7** illustrates CMA image maps for the P7 wet and dry area. The CaO concentration is low in the range approximately 3−6 mm from the surface, is high in the surface layer (approx. 1−3 mm), and rapidly declines in the extreme surface layer. In contrast, the $SiO_2$ concentration is high in the range 3−6 mm from the surface, decreases in the range 1−3 mm, and increases in the extreme surface layer. This result is identical compatible with the results of dissolution tests of cement paste using carbon dioxide solution conducted by Revertegat et al. [10] over a period of three years. That is, calcium dissociates from calcium silicate hydrate in the range 3−6 mm from the surface and transfers toward the surface. This, calcium carbonate is present 1−3 mm from the surface due to carbonation, calcium dissolves in the extreme surface layer, and silica gel remains. Judging from the results of a survey by Taylor and Newbury [11], the $CaO/SiO_2$ mole ratio of calcium silicate hydrate generated from portland cement is 2.5 or less, with a lower limit estimated at 1.43. It is considered that the $CaO/SiO_2$ mole ratio exceeds 2.5 due primarily to the effect of calcium hydroxide and calcium carbonate, in addition to the impact of monosulphate and calcium aluminate hydrate. In addition, it is possible that below 1.43 there is susceptibility to the impact of calcium silicate hydrate with a low $CaO/SiO_2$ mole ratio. The $CaO/SiO_2$ mole ratio distribution indicates that it is 1.0−1.35 in the range 3−6 mm from the surface, above 2.5 at depth of 1−3 mm, and 0.6 or below in the extreme surface layer. This can be regarded as resulting from a

decrease in the $CaO/SiO_2$ mole ratio of calcium silicate hydrate due to the dissociation of calcium, the presence of calcium carbonate and further reduction of the $CaO/SiO_2$ mole ratio due to dissociation of calcium and the generation of silica gel, respectively.

(6) SEM−EDS

**Photos 2−10** are typical SEM images. At 50 mm, the calcium hydroxide is platey and has a layered structure (A), and calcium silicate hydrate is Type III spherical (B) (**Photo 2**). At 10 mm, however, calcite is generated due to carbonation (**Photo 3**). Calcium silicate hydrate has a rough surface (**Photo 4**), and further progress of carbonation causes crystal bars to form (**Photo 5**). There are cases in which spherical calcium silicate hydrate decreases in quantity and more root−shaped crystals are seen (**Photo 6**). Next to the crystals, small spherical particles primarily consisting of silica are confirmed. These spherical particles are thought to be generated by the decomposition of calcium silicate and are thought to ultimately change into silica gel (**Photo 7**). Furthermore, calcium dissociates from the root−shaped crystals, which then change into needle crystals with silica and alumina as the major components (**Photo 8**). **Photo 9** shows spherical vaterite generated by carbonation. These observation results reveal that calcium silicate hydrate changes into crystals whose major components are silica and alumina because of carbonation.

At a depth of 10 mm in the Beam 3, gypsum most likely generated by the decomposition of monosulphate caused by carbonation, was confirmed present (**Photo 10**). This result also backs up reports by Stark and Ludwig [8].

(7) Pore size distribution

**Figure 8** presents the pore size distribution with a diameter of 3 nm−10 μm. A pore diameter of 10 nm is set as the boundary between gel and capillary pores in conformity with the classification by Stark and Ludwig [7].

← Concrete surface

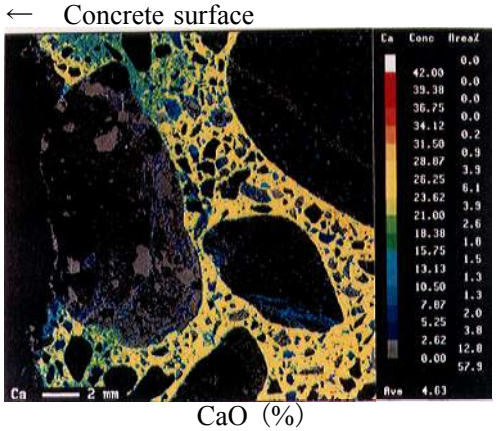

CaO (%)

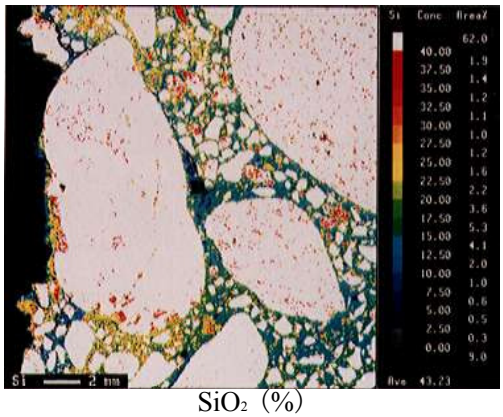

$SiO_2$ (%)

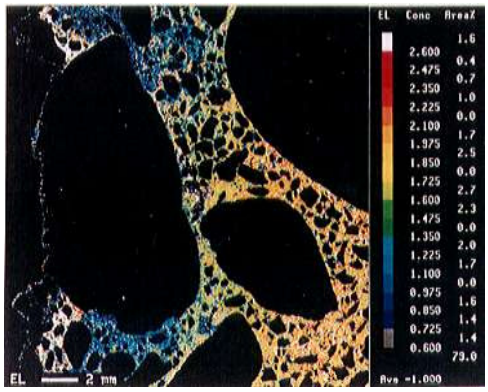

$CaO/SiO_2$ mole ratio

**Fig. 7** CMA image maps

Suryavanshi and Swamy [12] referred to pores 100 nm and larger as macropores and reported that macropores decrease as calcium carbonate is deposited on them due to carbonation. Further, Penttala and Matala [13] have reported that carbonation reduces the number of gel pores, enlarges the pore structure, and causes pore opening. These reports lead to the prediction that gel pores and macropores are reduced by carbonation. A comparison of the region at 10 mm and inner region indicates that macropores decrease only in the Beam 3, while in other areas they increase. However, gel pores decrease at 10 mm of four cores and pores 10−100 nm increase. Furthermore, pores 100 nm and larger also increase in the Beam 5 and the P7 in−air area. This indicates that further progress of carbonation causes macropores to increase in number. The differences in pore structure, expect for P7 wet and dry area, indicate the same tendency with the differences of average carbonation depth. On the other hand, pores between 10 and 100 nm significantly increase in the P7 wet and dry area, and pores 100 nm and larger also increase. This is thought to be caused by the combined action of carbonation and calcium dissociation into flowing water, considering the fact that the average depth of neutralization is less in the P7 wet and dry area than in the Beam 5.

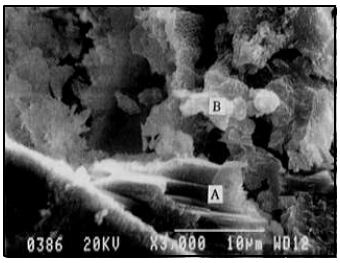


**Phot. 2** Beam 1（50 mm）

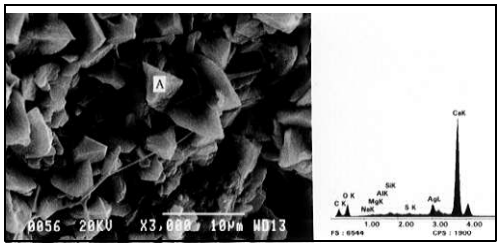


**Phot. 3** P7 in-air（10 mm）

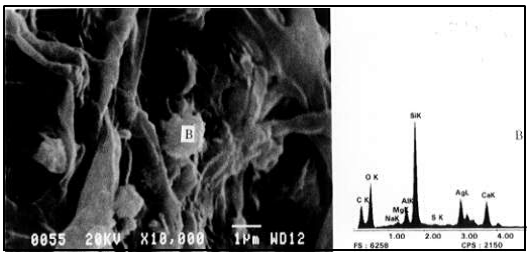


**Phot. 7** P7 in-air（10 mm）

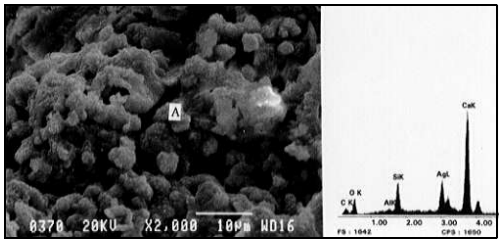


**Phot. 4** Beam 3（10 mm）

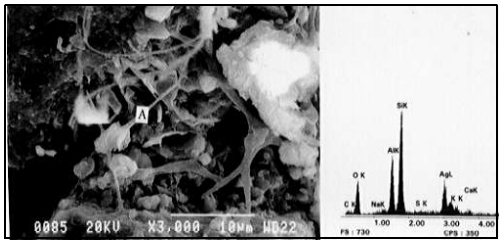


**Phot. 8** Beam 5（10 mm）

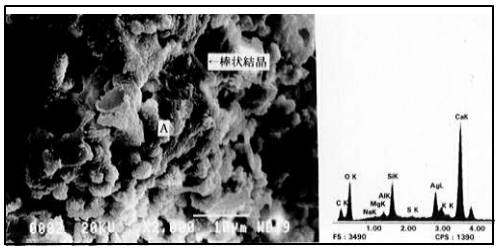


**Phot. 5** Beam 5（10 mm）

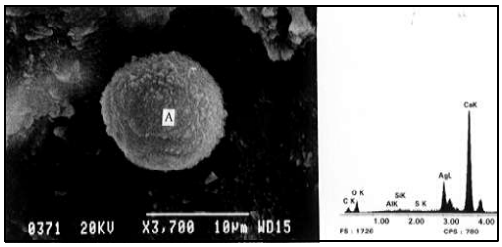


**Phot. 9** Beam 3（10 mm）

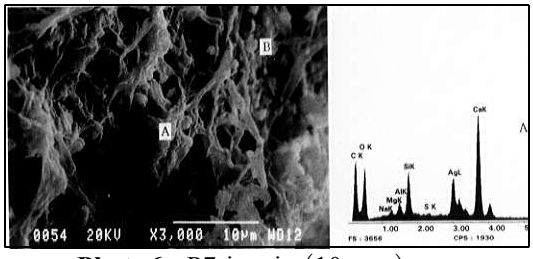


**Phot. 6** P7 in-air（10 mm）

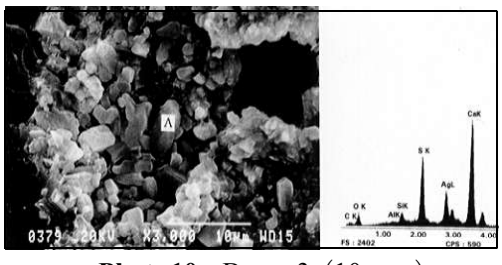


**Phot. 10** Beam 3（10 mm）

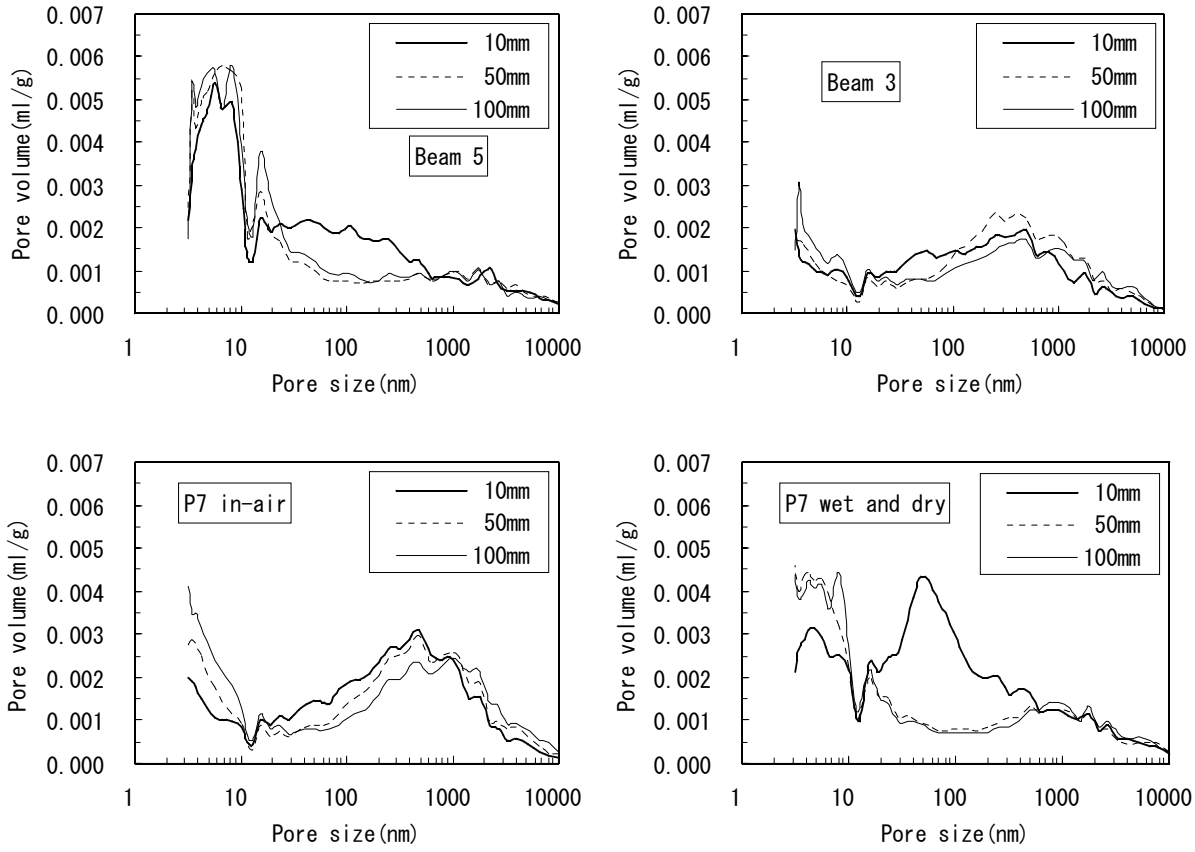


**Fig.8** Pore size distribution

(8) Freeze-thaw resistance

**Table 9** gives the relationship between durability factor and void texture (spacing factor, air content, and pore volume of 100 nm – 1 μm by the mercury penetration method) in freeze-thaw tests.

**Table 9** Relationship between durability factor and air void system

| | Durability index (%) | Spacing factor (μm) | Air content (%) | Pore volume at 100 mm from surface (100 nm – 1 μm) (ml/g) |
|---|---|---|---|---|
| Beam 3 | 6 or below | 899 | 1.64 | 0.0164 |
| P7 in-air | 6 | 440 | 0.50 | 0.0204 |
| P7 wet and dry | 21 | 432 | 0.65 | 0.0109 |
| P7 underwater | 21 | 603 | 0.45 | 0.0094 |
| Abutment | 21 | 604 | 2.30 | 0.0075 |

Specimens from Beam 4 collapsed after 30 cycles of freezing and thawing. This corresponds closely with the results of freezing and thawing tests of below 25 cycles and 83 cycles on inland reinforced concrete bridges (13.8-17.3 $N/mm^2$ in compressive strength) constructed in the same period as the first Tokachi Bridge [14][15].

The concrete of piers and abutments, which was often exposed to water during the service life, barely survived freeze-thaw tests lasting about 200 cycles, and has little freeze-thaw resistance. Its durability factor is just of 21%.

Cores were sampled from the pier P7's in−air, wet and dry, and underwater areas to investigate the impact of environmental conditions, but no marked differences in freeze−thaw resistance were observed.

Although it is thought that the desirable spacing factor is 250 μm or less, spacing factors of all cores were 400 μm or greater, which suggests low freeze-thaw resistance and is consistent with the freeze−thaw test results. The air content was also between 0.45 and 2.3%, which is much lower than the 4−6% of AE concrete, suggesting that it is non−AE concrete.

On the other hand, the pores that are harmful to freeze-thaw resistance are those 100 nm−1 μm in diameter, and water contained in these pores freezes and expands, destroying the hardened structure. Therefore, the pore volume in this range is considered to affect resistance. As shown in **Table 9**, the volume of pores 100 nm−1 μm at a depth of 100 mm from the core surface correlates with durability index, indicating that the pore volume in this range exerts an influence on resistance.

The effectiveness of AE agents was confirmed in the United States in 1932, and they were introduced into Japan in 1948. Therefore, concrete made when this bridge was constructed can not be expected to have freeze−thaw resistance. Nevertheless, actual bridges sustained little frost damage. Back then, countermeasures were taken; such as covering locations susceptible to frost damage with brick or stone facings. The same applied to the Tokachi Bridge, whereby Tokachi granite with a water absorption of 0.35% was used for the upper parts of curbing etc. that were susceptible to frost damage. As a result, the Tokachi Bridge remained immune to major frost damage. As indicated by these results, blocking the influx of water with stone or similar was an effective way to prevent frost damage.

## 7. CONCLUSIONS

The following points were clarified as a result of this study:

( 1 ) The cement was coarse, with the maximum grain size of 200−300 μm.

( 2 ) The cement in beam, slab, and pier concrete had different clinker burning conditions. Although the clinker burning conditions of beam and slab were favorable, clinker burning and cooling conditions of the pier were uneven. These differences appear in the form of differences in concrete texture and strength of the superstructure and piers.

( 3 ) The cement had a clinker composition consisting of small amount of alite and large amount of belite, and was close to a modern moderate−heat portland cement.

( 4 ) A common ingredient of the concrete was volcanic ash derived from fine aggregate, and this caused noticeable pozzolanic reactions with cement.

( 5 ) The compressive strength of the concrete increased by 1.8−2.0 times during the 50−odd years of service life. This marked increase in compressive strength is results from the coarse cement and large proportion of belite. As similar increases in strength are observed even in cement made with unfavorable burning conditions, it is clear that long−term pozzolanic reactions of volcanic ash also had an impact.

( 6 ) The average neutralization rate coefficient was **K**=3 mm/year$^{1/2}$ or below, except for the outer beam (Beam 5). This is comparable to manufacture to precast concrete standards, indicating that the construction work was good.

( 7 ) Although carbonation caused the generation of calcite, vaterite was also generated in some locations. Vaterite was found in locations where large amounts of calcite was generated. Furthermore, gypsum was generated by the decomposition of monosulphate, and gypsum triggers the generation of ettringite. The locations where vaterite and/or gypsum were identified are deteriorating more rapidly than other areas.

( 8 ) Calcium silicate hydrate with a low $CaO/SiO_2$ mole ratio is generated by carbonation, and further

carbonation generates silica gel. Silica gel does not function as a cement binder and its presence demonstrates significant deterioration. If areas with a $CaO/SiO_2$ mole ratio of below 1.43 on CMA result are regarded as deteriorated, the maximum range is approximately 6 mm from the surface.

( 9 ) Crystal morphology and components gradually changed during the progress of carbonation of calcium silicate hydrate, and crystals consisting mainly of silica and alumina were generated. This phase refers to a deteriorated condition prior to the generation of silica gel and alumina gel.

(10) Due to carbonation, gel pores 10 nm and smaller and macropores 100 nm and larger decrease while pores 10−100 nm increase. Further carbonation causes pores 100 nm and larger to increase as well. The increase in pores 100 nm and larger is regarded as indicating the deterioration of calcium silicate hydrate and monosulphate.

(11) Degree of carbonation was most advanced in the P7 wet and dry area, because calcite and vaterite were most existed at depth of 10 mm. On the other hand Beam 5 had the largest depth of carbonation, because loosening of texture of concrete by freeze−thaw action accelerated carbonation. In general the outer upstream beam (Beam 5) was in the most sever environment.

(12) The concrete was non−AE concrete with little freeze−thaw resistance. As the actual bridge sustained little frost damage, however, it is considered that minimizing the water supply to the concrete by improved drainage, use of stone facing, and other measures were effective in preventing frost damage.

(13) Deterioration due to neutralization, etc. was limited to the surface layer alone. As of now, the deterioration is minor, but durability needs to be confirmed through long-term exposure tests in the future.

**Acknowledgments**

Authors received full cooperation with the surveys from Mr. Masayuki Yamagami and Mr. Fumiyoshi Koyauchi of Obihiro Road Office, Hokkaido Development Bureau. With regard to the microscope observations of clinker, authors received guidance from Mr. Tetsuya Katayama of Kawasaki Geological Engineering Co., Ltd. Authors would like to express our great appreciation to them.

**References**

[ 1 ] Hideo Yokomichi: Report and Research on the Kasai Bridge Part 1: Construction Outline for the Kasai Bridge, Journal of the Japan Society of Civil Engineers, Vol.28, No.7, pp.599−631, 1942 (in Japanese)
[ 2 ] Hideo Yokomichi: Reports and Studies on Kasai−bashi (Part 6): Execution of Reinforcement and Bridgebody Concrete−Works, REPORT OF THE CIVIL ENGINEERING RESEARCH INSTITUTE, No.3, pp.20−44, 1948 (in Japanese)
[ 3 ] Shoichiro Nagai and Yaroku Fukushima: Research on Construction Materials, Series 1, Cement Materials (Part 1), Maruzen Publishing Co., 1948 (in Japanese)
[ 4 ] Schiessl, P.: Influence of the composition concrete on the corrosion protection of the reinforcement, ACI, SP100.82, pp.1633−1650, 1987
[ 5 ] Roy, S.K., Poh Kong, and Northwood, D.O.: The carbonation of concrete structures in the tropical environment of Singapore and a comparison with published data for temperate climate, Magazine of Concrete Research, Vol.48, No.177, Dec., pp.293−300, 1996
[ 6 ] Menzies, J., Moore, J., and Currie, R.: The durability of structural concrete in modern buildings in the United Kingdom, ACI, SP100.11, pp.142−167, 1987
[ 7 ] Stark, J. and Ludwig, H.M.: Freeze−thaw and freeze−deicing salt resistance of concrete containing cement rich in granulated blast furnace slag, ACI MATERIALS JOURNAL, January−February, pp.47−55, 1997
[ 8 ] Stark, J. and Ludwig, H.M.: The role of phase conversions in the hardened cement paste when concrete is attacked by freeze−thaw and freeze−thaw with de−icing salt, ZKG INTERNATIONAL,

pp.648−663, Nr.11, 1996
[ 9 ] Naohiro Nishikawa and Kazutaka Suzuki: Carbonation of Calcium Silicate Hydrate, Cement & Concrete, No.528, pp.32−39, 1991 (in Japanese)
[10] Revertegat, E., Richet, C., and G gout, P.: Effect of pH on the durability of cement pastes, Cement and Concrete Research, Vol.22, pp.259−272, 1992
[11] Taylor, H.F.W. and Newbury, D.E.: An electron microprobe study of a mature cement paste, Cement and Concrete Research, Vol.14, pp.565−573, 1984
[12] Suryavanshi, A.K. and Swamy, R.K.: An evaluation of controlled permeability formwork for long−term durability of structural concrete elements, Cement and Concrete Research, Vol.27, pp.1047−1060, 1997
[13] Penttala, V.E. and Matala, S.P.: Strength and composition changes in carbonated GBFS and OPC mortars during extended water curing, Proceedings of the International Conference Under Severe Condition, Vol.2, pp.1183−1194, 1995
[14] Toshitaka Ohta, Takashi Fujii and Shizuo Maekawa: Investigation on Thirty−odd−year−old Reinforced Concrete Bridges, Cement & Concrete, No.290, pp.15−20, 1971 (in Japanese)
[15] Toshitaka Ohta: Frost Damage and Repair, Concrete Journal, Vol.31, No.7, pp.79−82, 1993 (in Japanese)